

Automated Lesion Segmentation of Stroke MRI Using nnU-Net: A Comprehensive Exploration of Acute and Chronic Lesions

Tammar. Truzman*, Matthew A. Lambon Ralph & Ajay D. Halai

MRC Cognition and Brain Sciences Unit, University of Cambridge, Cambridge, UK

[*Tammar.truzman@mrc-cbu.cam.ac.uk](mailto:Tammar.truzman@mrc-cbu.cam.ac.uk)

Highlights:

- nnU-Net models achieved lesion-segmentation performance within known human agreement ranges for both acute and chronic stroke.
- DWI consistently outperformed FLAIR in acute stroke lesion segmentation.
- Model performance improved with larger chronic T1-weighted datasets.
- Lesion laterality did not impact segmentation accuracy or generalisability.
- Lesion volume was a key determinant: while generalisation required a broad lesion volume distribution during training, very small lesions remained challenging to segment.
- Models trained on high-quality MR scans generalised well to lower-quality data, but not vice versa.

Abstract

Accurate and generalisable segmentation of stroke lesions from magnetic resonance imaging (MRI) is essential for advancing clinical research, prognostic modelling, and personalised interventions. Although artificial intelligence, including deep learning, has substantially improved automated lesion delineation, many existing models are optimised for narrow imaging contexts and generalises poorly to independent datasets, modalities and stroke stages. Here, we systematically evaluated stroke lesion segmentation using the nnU-Net framework across multiple heterogeneous, publicly available MRI datasets, spanning acute and chronic stroke. Models were trained and tested on diffusion weighted imaging (DWI), fluid-attenuated inversion recovery (FLAIR), and T1-weighted MRI, and were evaluated on fully independent datasets. Across acute and chronic stroke, our models achieved robust generalisation, with segmentation accuracy approaching reported inter-rater reliability for manual annotations. Performance varied systematically as a function of imaging modality and training data characteristics. For acute stroke, models trained on DWI consistently outperformed those trained on FLAIR, with only marginal, but significant, gains from multimodal combination. In chronic stroke, increasing training set size improved performance with diminishing returns beyond several hundred cases. Lesion volume emerged as an important determinant of accuracy: smaller lesions were

consistently harder to segment, and models trained on restricted volume ranges generalised poorly. Furthermore, MRI image quality constrained model generalisability: models trained on lower-quality scans transferred poorly, whereas those trained on higher-quality data generalised well even to noisier images. Inspection of failed cases revealed that discrepancies between model prediction and reference masks were often attributable to inconsistencies or limitations in manual annotations, highlighting how variability in current gold standard labels constrains performance. Together, these findings demonstrate that automated lesion segmentation can achieve comparable levels to humans, while identifying key factors that govern generalisability. By leveraging open datasets, open-source algorithms, and code, this work provided practical guidance for developing robust, transparent, and clinically relevant stroke lesion segmentation tools.

Keywords: Stroke; Lesion segmentation; Deep learning; nnU-Net; MRI

1. Introduction

Stroke remains a leading cause of death and long-term adult disability worldwide, with its prevalence and societal impact increasing in aging populations (Feigin et al., 2017). Brain damage following stroke is highly heterogeneous, and different neuroimaging modalities are informative at different stages of the disease; for example, perfusion-based imaging in the acute phase and structural imaging in the chronic phase. Rapid and accurate identification of stroke lesions is therefore essential not only for clinical diagnosis, prognosis, and disease monitoring (Liu et al., 2020; Luo et al., 2024), but also for advancing research in stroke neuropsychology and recovery. Lesion-symptom mapping has been central to stroke aphasia research since classical post-mortem studies by Broca and Wernicke, and contemporary neuroimaging now enables non-invasive, high-resolution three-dimensional reconstruction of damaged tissue. This has facilitated the development of quantitative approaches such as voxel-based lesion symptom mapping (VLSM) (Bates et al., 2003) and multivariate lesion-symptom methods (DeMarco & Turkeltaub, 2018; Zhang et al., 2014). Furthermore, precise lesion identification can support participant stratification in targeted therapeutic trials (Iqbal et al., 2024) and the identification of imaging biomarkers predictive of post-stroke recovery trajectories (Bowren et al., 2022; Iorga et al., 2021; Kristinsson et al., 2021; Price, 2010; Wilson et al., 2023).

Despite its importance, accurate lesion identification remains challenging due to substantial variability in lesion appearance, imaging protocols, and tissue characteristics across patients and centres (Chauhan et al., 2019). Manual lesion tracing is considered the gold standard but is time-consuming, requires specialised expertise, and is subject to inter- and intra-rater variability (Ito et al., 2019; Nazari-Farsani et al., 2020). Even under standardised protocols, inter-rater reliability for chronic lesions is approximately .72 and intra-rater reliability .84 (Liew et al., 2018; Lo et al., 2022), motivating the development of automated methods to improve efficiency, objectivity, and reproducibility (Sharma et al., 2010).

In the first wave of development, several automated or semi-automated approaches were proposed (De Haan et al., 2015; Griffis et al., 2016; Pustina et al., 2016; Seghier et al., 2008); however, generalisation to external datasets was limited, particularly when applied to data from diverse sites, scanners, and stroke populations. Ito et al., (2019) compared four automated methods and found that the best algorithm (using LINDA; Pustina et al., 2016)) achieved a median Dice coefficient (proportion of overlap between ground truth and predicted lesion) of .5 on stroke data collected worldwide. This performance falls below reported inter-rater reliability (cf. .72), substantially limiting its utility for clinical and research application.

More recently, advances in artificial intelligence, particularly deep learning, have led to substantial improvements in automated stroke lesion segmentation. However, reported model accuracy must be interpreted in light of several critical considerations. First, lesion appearance evolves markedly over time following stroke. Acute lesions are dominated by hypoperfusion and cytotoxic oedema, whereas chronic lesions reflect tissue loss, cavitation and gliosis. This temporal evolution directly determines which neuroimaging modalities are most informative for lesion detection, which, in turn, influences algorithms performance (Baaklini & Valdés Hernández, 2025a; Hernandez Petzsche et al., 2022). Consequently, some approaches have developed models tailored to specific post-stroke phases (Ahmed et al., 2024), while others have sought to build models that generalise across time points (Chalcroft et al., 2025). Second, the heterogeneous nature of stroke lesions often necessitates multi-modal imaging, introducing a trade-off between models optimised for specific modalities (or sets) (Ahmed et al., 2024) and modality-invariant models intended to be flexible across diverse protocols

(Chalcroft et al., 2025). Increased flexibility may improve applicability but can come at the cost of reduced segmentation accuracy. Finally, evaluation strategies critically influence conclusions about generalisability. While random training, validation and test sets splits within a dataset are common, they may overstate real-world performance. In contrast, validation on independent datasets collected at different sites and scanners provides a stringent and clinically meaningful test. This distinction is evident in prior work: Ahmed et al. (2024) reported high Dice coefficient (.82) using held-out cases from ATLASv2 (S.-L. Liew et al., 2018), whereas Chalcroft et al. (2025) demonstrated marked performance degradation when models were required to generalise across datasets, modalities, or stroke stages.

In summary, while recent studies demonstrate considerable promise, there remains a clear need for models that can reliably segment both acute and chronic lesions with uni- or multi-modal imaging, and that are rigorously evaluated on independent datasets. Widespread adoption of automated approaches will depend not only on high performance, but also on transparency, open availability of models and code, and feasibility of deployment by users without specialist expertise in computer science.

In the current study, we utilise a streamlined and robust implementation of the original U-Net convolutional neural network architecture (CNN; Ronneberger et al., 2015), specifically the “no-new-U-Net” (nnU-Net; Isensee et al., 2020). nnU-Net is a fully automated, self-configuring framework that adapts network architecture and training parameters to the dataset at hand. Its strength lies in the end-to-end automation of the segmentation pipeline - from pre-processing, model configuration, training, inference and post-processing, while retaining flexibility for expert users where needed. Variants of nnU-Net have consistently achieved strong performance across diverse clinical imaging tasks (Baaklini & Valdés Hernández, 2025b; Jeong et al., 2024). Using nnU-Net, we systematically evaluated the performance and generalisability of automated stroke lesion segmentation across multiple openly available datasets containing manually delineated acute and chronic stroke lesions. Our primary aim was to develop models capable of reliably segmenting lesions across both time points, achieving performance approaching reported levels of human inter-rater agreement.

Beyond establishing strong baseline performance, the availability of multiple heterogeneous datasets allowed us to investigate key determinants of model generalisation. For acute lesion segmentation, we tested whether multimodal models would outperform unimodal models by integrating complementary information about tissue injury. For chronic lesion segmentation, we examined the effects of: (i) training dataset size; (ii) lesion spatial distribution; (iii) lesion volume distribution; and (iv) MRI scan quality in both training and test data. Consistent with general deep-learning principles, we hypothesised that larger and more diverse training datasets would improve generalisation.

All trained models, code, and documentation are openly shared to promote transparency, reproducibility, and community-wide development, and are available at <https://github.com/AjayHalai/Lesion-Segmentation-nnUNet>.

2. Methods

2.1. Datasets and Preprocessing

We used five independent stroke MRI datasets to evaluate the generalisability of nnU-Net for acute and chronic lesion segmentation. Each dataset included manually delineated lesion masks generated by experts on modality-appropriate sequences, which served as the ground truth. Figure 1a–e shows lesion spatial distribution and lesion volume profiles for each dataset.

2.1.1 Acute Stroke Datasets

(I) Stroke Onset Optimization Project (SOOP)

The SOOP dataset (N = 1456; Absher et al., 2024) comprises acute ischemic stroke cases with high-resolution T1-weighted (T1w) MRI, fluid-attenuated inversion recovery (FLAIR), trace diffusion-weighted imaging (DWI) and apparent diffusion coefficient (ADC) maps. Imaging was acquired within 48 hours of admission. Lesions predominantly involved the middle cerebral artery (MCA) territory, spanning cortical and subcortical regions across both hemispheres. Manual segmentation was performed on combined DWI–ADC images by three trained neuroscientists using MRIcroGL (Rorden & Brett, 2000). In cases with multiple infarcts, all lesions were merged into a single binary mask.

(II) Ischemic Stroke Lesion Segmentation (ISLES)

The ISLES dataset (N = 250; Hernandez Petzsche et al., 2022) includes DWI, ADC and a mixture of high- and low-resolution FLAIR scans acquired 1–3 weeks post-stroke. Data were collected from multiple sites and scanners, using 1.5T and 3T Philips or Siemens MRI systems. Lesions primarily involved the MCA territory, with approximately one quarter occurring in infratentorial regions and showing mixed hemispheric involvement. Segmentation followed a hybrid pipeline. First, a 3D U-Net algorithm (Çiçek et al., 2016) initially trained on DWI images ($b = 1000 \text{ s/mm}^2$) stemming from one of the centres, was used to generate initial lesion masks. These masks were then manually corrected by medical students using ITK-SNAP (Yushkevich & Gerig, 2017) or 3D Slicer (Fedorov et al., 2012). The masks were reviewed by neuroradiology residents and verified by senior neuroradiologists. Final masks were generated through joint inspection of DWI, ADC, and FLAIR. All lesion components were merged into a single binary mask per case.

2.1.2 Chronic Stroke Datasets

(III) Anatomical Tracings of Lesions After Stroke (ATLAS v2.0)

ATLAS v2.0 (N = 655; Liew et al., 2022; Liew et al., 2018) comprises chronic stroke cases (≥ 180 days post-stroke) with high-resolution T1w MRI and manually delineated lesion masks, pooled across 33 research cohorts. Imaging was acquired on 1.5T and 3T MRI scanners with heterogeneous acquisition parameters. The dataset predominantly consists of single-lesion cases (61.9%), with lesions distributed across cortical and subcortical regions and both hemispheres. Lesions were traced in MRIcron and ITK-SNAP using slice-by-slice manual delineation with optional interpolation for large lesions. Annotators received structured neuroanatomical training and adhered to detailed lesion-tracing guidelines (Liew et al., 2022). All segmentations underwent multi-stage quality control, including review by trained raters and consensus resolution with a neuroradiologist. All lesion components were merged into a single binary mask.

(IV) Aphasia Recovery Cohort (ARC)

The ARC dataset (N = 228; Gibson et al., 2024) includes individuals with chronic post-stroke aphasia after left-hemisphere infarcts, scanned on average $\geq 1,138$ days post-stroke (SD = 1,327). All T1w scans were acquired on Siemens 3T MRI systems (Trio and later Prisma) across multiple studies, resulting in variability in acquisition parameters. Lesions predominantly affected left MCA territory and were

mainly cortical. Although multi-modal imaging (including T2-weighted, DWI and functional MRI) is available for subsets of this cohort, only T1w images were used in the present study to ensure consistency with other chronic datasets. Lesion masks were manually delineated by an expert on the T2-weighted images from the first scanning session.

(V) Cambridge Cognitive Neuroscience Research Panel (CCNRP)

The CCNRP dataset (N = 204) includes individuals with a broad range of focal brain lesions. Based on clinical diagnosis, approximately 36% of cases reflected stroke-related injury (e.g., ischemic infarct, haemorrhage, aneurysm, or AVM-related events), 53% reflected tumour-related pathology (e.g., meningioma, glioma, cavernoma, and other neoplasms or tumour resection), and the remaining 11% represented other aetiologies, including epilepsy surgery, encephalomalacia, and infections. Lesions exhibited heterogeneous anatomical distributions, spanning cortical and subcortical regions across both hemispheres. All patients were scanned with high-resolution T1w MRI, and lesions were manually delineated by a single expert neurologist. Scans and corresponding manual segmentations are available at [OpenNeuro](https://openneuro.org/datasets/CCNRP).

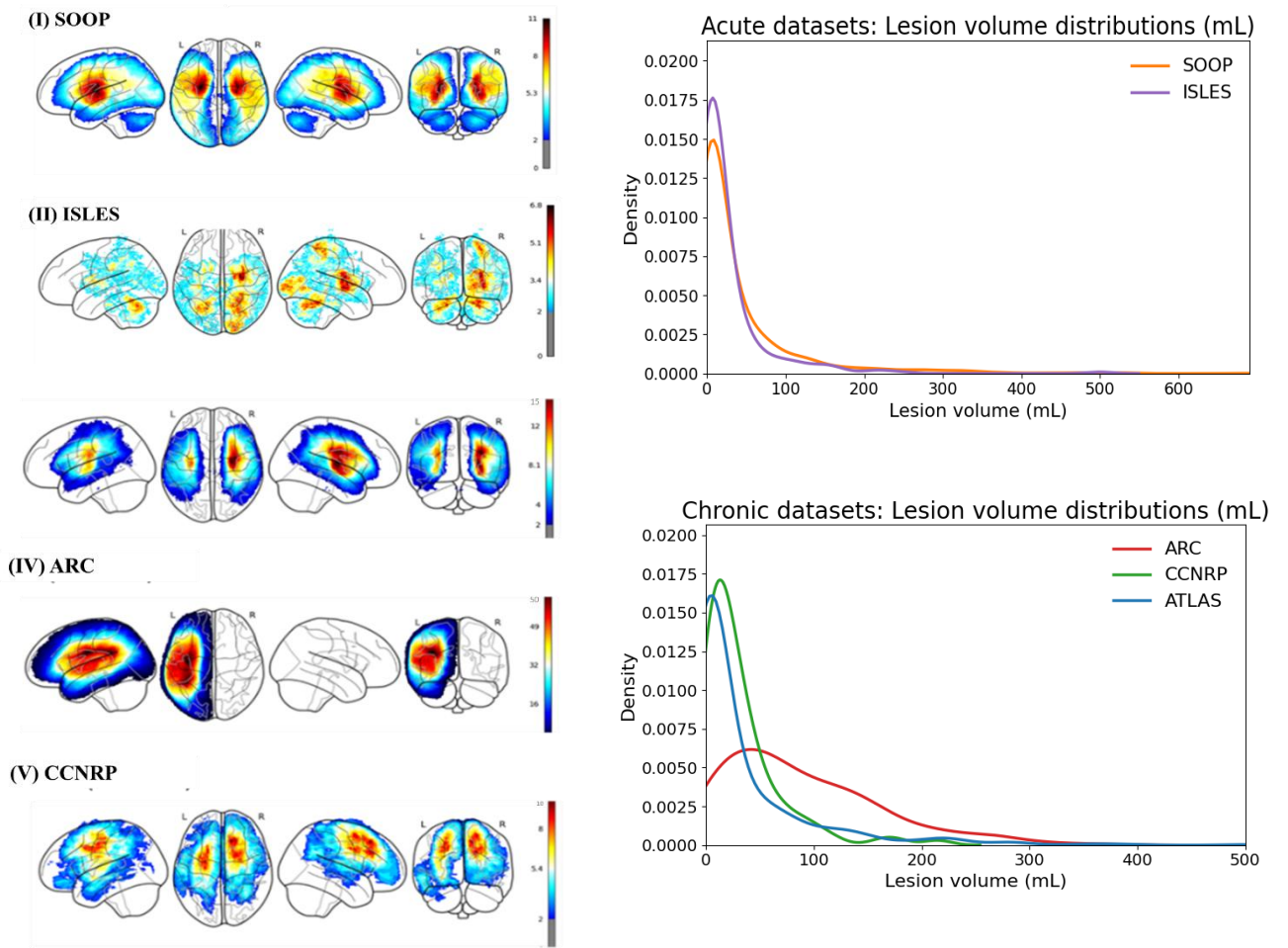


Figure 1. Lesion topography and volume distributions across datasets.

Left panel: Glass-brain lesion overlap maps show the number of participants with a lesion at a given location. The maximum overlap for each dataset is indicated on the colour bar (SOOP = 11, ISLES = 6, ATLASv2 = 12, ARC = 49, CCNRP = 8).

Right panel: Kernel density curves of lesion volume (mL) computed from the binary lesion masks for each dataset. Acute lesion volumes (top) were derived from DWI-based masks, whereas chronic lesion volumes (bottom) were derived from T1-weighted masks.

2.2. nnU-Net Architecture

All segmentation models were implemented using the nnU-Net framework (v2.3.1; Isensee et al., 2020)). Analyses were conducted on a Linux server equipped with five GPUs (3 × NVIDIA A30, 24 GB; 2 × NVIDIA L40S, 48 GB). We followed the standard nnU-Net workflow, beginning with automated preprocessing (*nnUNetv2_plan_and_preprocess*), which included metadata extraction, Z-score intensity normalisation, and automatic generation of configuration plans for both the standard full-resolution 3D U-Net (3d_fullres) and a residual-encoder variant (3d_fullres_resenc). To reduce computational burden, we did not train 2D, 3d_lowres, or cascade models. All models were trained

using the default nnU-Net settings; a complete list of parameters is provided at <https://github.com/AjayHalai/Lesion-Segmentation-nnUNet>.

For acute stroke datasets, diffusion inputs consisted of paired DWI and ADC maps, which were always provided together to nnU-Net as a two-channel input (hereafter referred to as DWI). In multimodal experiments (DWI+FLAIR), each sequence was included as a separate image channel. For chronic stroke datasets, models were trained using single-channel T1w images.

Initial model training and internal evaluation (*nnUNetv2_train*) was performed using five-fold cross-validation for each training dataset, using the default loss function (a combination of Dice coefficient and cross-entropy loss) to optimise both spatial overlap and voxel-wise classification. As two architectural configurations were trained per dataset, we used *nnUNetv2_find_best_configuration* to identify the optimal model (either separate or ensemble) based on mean cross-validation Dice scores. The selected model was subsequently applied to independent held-out test datasets (*nnUNetv2_predict*) followed by post-processing (*nnUNetv2_apply_postprocessing*) to remove small, disconnected components and enforce binary masks.

2.3. Evaluation Metrics

Following standard practice in medical image segmentation (Taha & Hanbury, 2015), performance was evaluated using the Dice coefficient and 95th percentile Hausdorff Distance (HD95). The Dice coefficient quantifies spatial overlap between predicted and reference lesion masks, with values ranging from 0 (no overlap) to 1 (perfect overlap). HD95 measures the boundary distance between predicted and reference segmentations and is less sensitive to extreme outliers. It was capped at 256 mm, corresponding to the maximum Euclidean distance within a 1 mm isotropic image grid. In addition, we computed a comprehensive set of voxel-wise and surface-based metrics, including intersection over union (IoU), full Hausdorff distance, mean surface displacement, confusion matrix derived measures, absolute volume difference, and lesion-level F1 score. These additional results are provided in Supplementary Table S1 but are not discussed further here for simplicity.

2.4. Statistical Analysis

All analyses were hypothesis-driven and focused on evaluating model performance and generalisability. For clarity, statistical inference is reported primarily on external validation datasets. Group comparisons of Dice and HD95 across experimental conditions were conducted using non-parametric Mann–Whitney U or Wilcoxon signed-rank tests as appropriate (two-sided, $\alpha = .05$). Bonferroni correction was applied where multiple comparisons were performed. Dataset-specific results are provided in the Supplementary Materials Table S1.

2.4.1. Best-Performing Model

We first addressed the central question of whether automated models can approach human-level reliability when evaluated on fully independent datasets for each time point (acute and chronic).

For acute stroke, the search space consisted of separate nnU-Net models trained for each modality configuration available within the SOOP and ISLES datasets (DWI, FLAIR, and multi-channel DWI+FLAIR). For chronic stroke, we similarly trained separate models on all T1w images from the ATLASv2, ARC, and CCNRP datasets. Within each time point, all trained models were evaluated on their respective held-out external test datasets, and the model achieving the highest external validation performance was selected as the best acute and chronic model, respectively.

2.4.2. Effect of Training Set Size (chronic T1w lesions)

To examine the effect of training size on segmentation, we trained nnU-Net models on three nested subsets of the ATLASv2 dataset ($n = 218, 436, 655$), randomly split without replacement. Model performance was evaluated on the held-out ARC and CCNRP datasets. Consistent with deep-learning principles, we expected accuracy to improve with larger training set size.

2.4.3. Effect of Lesion Laterality (chronic T1w lesions)

The ARC dataset contains exclusively left hemisphere (LH) lesions. Therefore, we examined whether lesion laterality in the training data influences model generalisation. We hypothesised that models trained on laterality-restricted datasets would reduce generalisability to datasets with heterogeneous lesion distributions. To test this, we stratified the ATLASv2 dataset into LH ($n = 205$),

right-hemisphere (RH; $n = 224$), and bilateral (BL; $n = 226$) subsets, trained separate models, and evaluated their performance on held-out ATLASv2 and CCNRP datasets.

2.4.4. Effect of Lesion Volume (chronic T1w lesions)

We examined the influence of lesion volume (normalised as % intracranial volume) on segmentation performance in two complementary ways. As an outcome measure, we assessed non-linear associations between lesion volume and Dice scores using Spearman correlations across all external validation tests. Additionally, we analysed performance for small lesions using two thresholds ($< 10 \text{ cm}^3$ and $< 20 \text{ cm}^3$) to determine whether volume effects persisted within these restricted size ranges. As a training feature, we first tested generalisation by training models on very small lesions ($< 5 \text{ cm}^3$; $n = 319$) or larger lesions ($> 5 \text{ cm}^3$ up to $\sim 400 \text{ cm}^3$; $n = 336$) from the ATLASv2 dataset. Each model was then evaluated on the alternate subset (small \rightarrow large; large \rightarrow small), as well as on the held-out ARC and CCNRP datasets. Secondly, given that ATLASv2 is heavily skewed toward smaller lesions, we tested whether a broader lesion-volume distribution improves performance. To do this, we constructed a volume-matched subset of ATLASv2 ($n = 204$) that approximated the lesion-volume distribution of CCNRP. A model trained on this volume-matched ATLASv2 subset was evaluated on CCNRP, and the previously trained CCNRP model was likewise evaluated on the matched ATLASv2 subset, allowing us to assess generalisation in both directions. Matching either dataset to ARC was not feasible due to the substantially larger and left-lateralised lesions present in the ARC dataset.

2.4.5. Effect of Image Quality (chronic T1w lesions)

Finally, we assessed whether differences in MRI quality contributed to variability in performance. Image quality metrics were extracted from T1w images using MRIQC (Esteban et al., 2017) for the three chronic datasets. MRIQC provides a broad set of quantitative measures that can be grouped into: 1) noise-related measures (e.g., contrast- or signal-to-noise ratio; CNR and SNR, respectively), 2) information-theoretic measures (e.g., foreground-background energy ratio and energy-focus criterion), 3) artifact-related measures (e.g., bias field intensity, artifact signal in air space, and white matter intensity), and 4) structural measures (e.g., blurriness, residual partial volume effects, intracranial volume, tissue probability maps overlapping with MNI template). A full description of these metrics is

provided in the original MRIQC publication. To reduce dimensionality and summarise latent qualities, we applied principal component analysis (PCA) with varimax rotation, retaining components with eigenvalues > 1 . Component scores were compared across datasets to evaluate systematic MRI quality and their potential contribution to model performance.

3. Results

Below, we report model performance results structured around the key hypotheses outlined above. Unless otherwise specified, external validation results are reported by pooling all cases across the relevant held-out test datasets for each comparison.

3.1 Best Performing Models: Acute and Chronic Lesions

Among the two highest-performing models, the SOOP-trained DWI+FLAIR model achieved the best segmentation accuracy (median Dice = .777; median HD95 = 2.45 mm) and showed a statistically significant improvement over the SOOP-trained DWI-only model (median Dice = .774; Wilcoxon $W = 11,464.5, p < .001$). Despite this difference, the DWI only model remains highly useful in practice given it requires fewer imaging data with minimal actual performance loss. Across all modality configurations, models trained using DWI consistently outperformed FLAIR models (all $p < .001$). Details of all models are shown in Supplementary Materials Table S1.

For chronic stroke, the best-performing model was the ATLASv2 model, which achieved a median Dice of .81 (HD95 = 4.20 mm) on ARC and .73 (HD95 = 5.10 mm). This model outperformed both the CCNRP and the ARC trained-models (all $p < .001$), See Table 1. Details of the winning models shown in Supplementary Table S1.

Taken together, these results demonstrate that nnU-Net can achieve performance on heterogeneous, independent datasets that falls within the range of published inter-rater reliability (Dice $\approx .72\text{--}.84$; (Hernandez Petzsche et al., 2022; Ito et al., 2019; Nazari-Farsani et al., 2020).

Upon inspecting individual cases we found that segmentation errors, reflected by low Dice and/or high HD95, arose from both model limitations and annotation inaccuracies. In some instances, low Dice reflected clear model failures, such as missing lesions. In other cases, discrepancies were

attributable to limitations in the ground truth annotations, including mislabelled voxels outside the brain, under-segmentation, or inconsistently defined lesion boundaries. These examples indicate that evaluation metrics may reflect a combination of model error and annotation noise. Representative examples are shown in Figure 2.

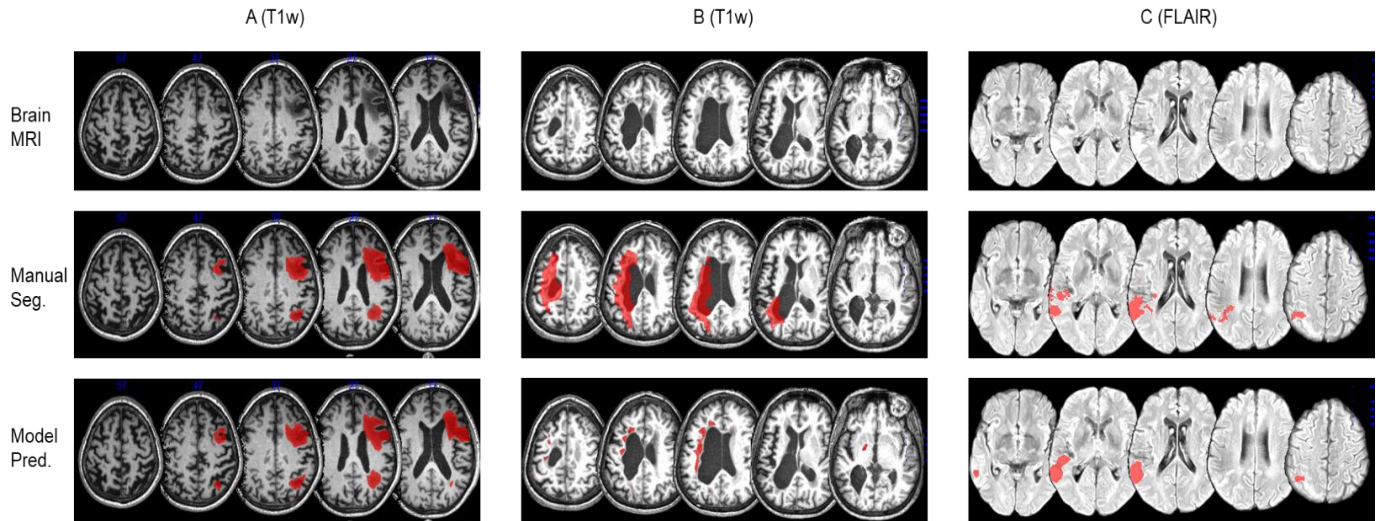


Figure 2. Segmentation examples of stroke lesions across datasets. For each case, axial images in MNI space are shown (top), manual lesion masks (ground truth; red) are overlaid (middle), and model predictions (red) are overlaid (bottom).

(A) Chronic T1w example (prediction ATLASv2 → CCNRP) showing a large cortical lesion with close agreement between prediction and manual mask (Dice = 0.90; HD95 = 2.25); (B) Chronic T1w (prediction ATLASv2 → ARC) showing a large lesion with poor overlap between prediction and manual mask (Dice = 0.30; HD95 = 21). Here, the discrepancy arises primarily from differences in lesion-definition conventions, e.g., whether enlarged ventricles or periventricular cerebrospinal fluid (CSF) should be considered part of the lesion; (C) Acute FLAIR (prediction SOOP FLAIR → ISLES FLAIR) showing a cortical lesion with moderate agreement between prediction and manual mask (Dice = 0.55; HD95 = 7.3), and highlighting the intrinsic challenges in FLAIR due to the presence of other hyperintense structures (e.g., white matter hyperintensities, oedema, or venous artefacts), which can resemble stroke lesions and contribute to both human and model ambiguity.

3.2 Effect of Training Set Size (chronic lesions; T1w)

Training set size had a clear monotonic effect on segmentation performance across external validation datasets. Dice scores increased significantly from the small ($n = 218$; median = .739) to the medium-sized model ($n = 436$; median = .762; $W = 20,220$, $z = -10.22$, $p < .001$). Consistent with this trend, the large model also significantly outperformed the medium model ($N = 655$; median = .774; $W = 34,050$, $z = -4.90$, $p < .001$). However, the magnitude of improvement was smaller, indicating diminishing returns beyond several hundred training cases. Dice score distributions are shown in Figure 3, with summary metrics in Table 1. For simplicity, results are pooled across both external validation datasets; dataset-specific results are provided in Supplementary Materials Table S1.

Table 1. Segmentation performance (median Dice and HD95) of nnU-Net models trained on chronic stroke lesions.

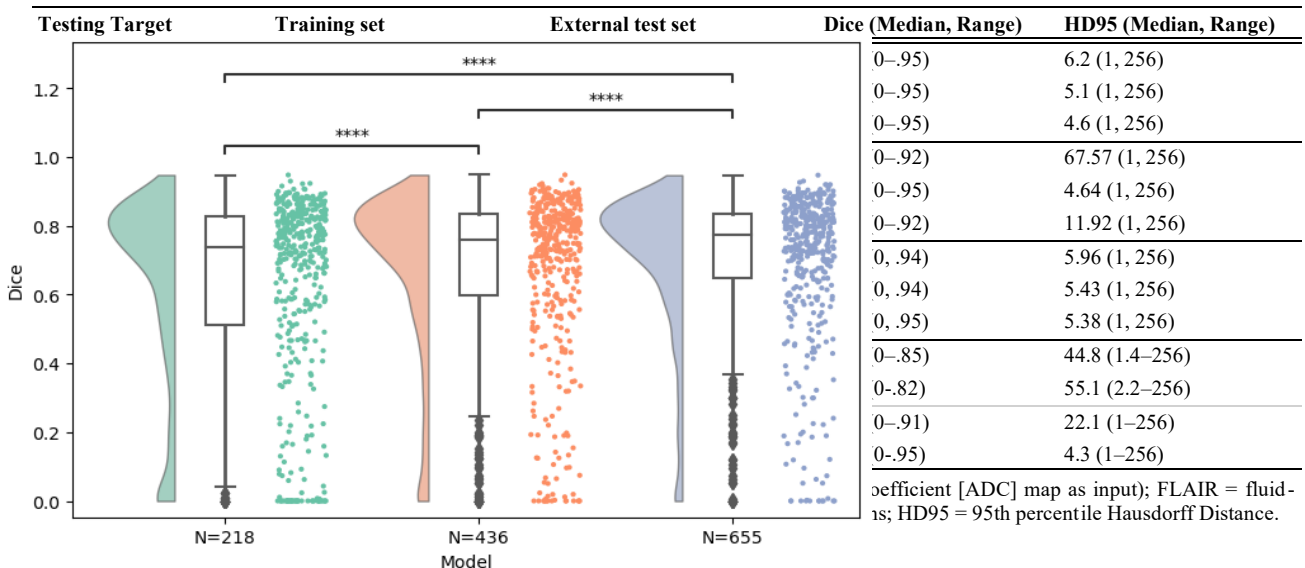


Figure 3. External-validation Dice scores for models trained on increasingly large subsets.

The X-axis indicates the ATLASv2 training subset size (N = 218, 436, 655), and the Y-axis shows the Dice coefficient obtained when these models were applied to the external ARC and CCNRP test sets (pooled results). Black horizontal lines mark median Dice values. ****p < .0001, Bonferroni-corrected.

3.3 Lesion Laterality Effects (chronic lesions; T1w)

The ARC trained model showed poor performance on external datasets (See Table 1), possibly due to the training data containing left sided lesions only. To test this, we trained separate models on laterality-restricted subsets of ATLASv2 (LH: $n = 205$; RH: $n = 224$; BL: $n = 226$), and compared their performance to the full ATLASv2 trained model that contained all cases (N = 655). Lesion volumes did not differ between LH and RH subsets ($p > .05$); however, both unilateral lesions were significantly larger than bilateral lesions (LH vs BL: $U = 6,109$, $p < .001$ and RH vs BL: $U = 7,723$, $p < .001$). All laterality-restricted models performed similarly with median Dice ranging from .74–.75, and no significant differences between models (Figure 4; Table 1). One exception was a small but significant reduction in performance for the LH model relative to the full ATLASv2 model (Dice = .74 vs. .77; $U = 83,390$, $p = .041$). Full dataset-specific results are provided in Supplementary Materials Table S1.

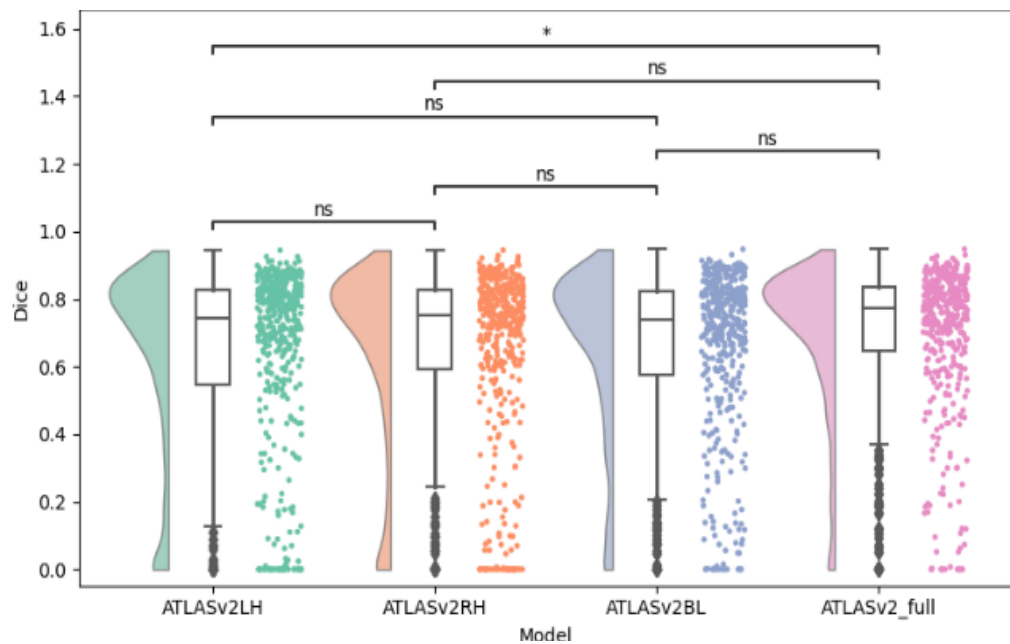


Figure 4. Dice score distributions for models trained on laterality-specific ATLASv2 subsets (LH, RH, BL) and the full ATLASv2 dataset. The X-axis indicates the training subset, and the Y-axis shows the Dice coefficient obtained on the pooled external ARC and CCNRP test sets (pooled results). Black horizontal lines mark median Dice values. $*p < .05$, Bonferroni-corrected.

3.4 Lesion Volume Effects (chronic lesions; T1w)

We next examined the influence of lesion volume on segmentation accuracy, considering lesion volume as both (i) a property of the test set affecting performance on individual cases, and (ii) a characteristic of the training set, influencing generalisation.

3.4.1 Test-set effects: smaller lesions are harder to segment

Spearman rank correlations revealed strong positive associations between lesion volume and Dice score across all models and external datasets ($r_s(202-653) = .49-.74$, all $p < .001$), indicating that larger lesions were segmented more accurately. An illustrative example for the ATLASv2 model is shown in Figure 5.

When analyses were restricted to small lesions ($\leq 20 \text{ cm}^3$), segmentation difficulty persisted. Lesions with poor segmentation accuracy (Dice $\leq .6$) were significantly smaller than those with better segmentation accuracy (Dice $> .6$; $U = 91-10,940$, all $p < .05$), indicating that lesion volume continued to influence performance even within this restricted range. In contrast, within the subset of very small

lesions ($< 10 \text{ cm}^3$), lesion volume no longer distinguished between well- and poorly segmented cases across all datasets (all $p > .05$). We plotted the lesion overlap map of the well- and poorly segmented lesions from the small lesion ($< 10 \text{ cm}^3$) but did not find obvious spatial patterns, although the poorly segmented lesions appeared more spatially dispersed (Supplementary Material Figure S1).

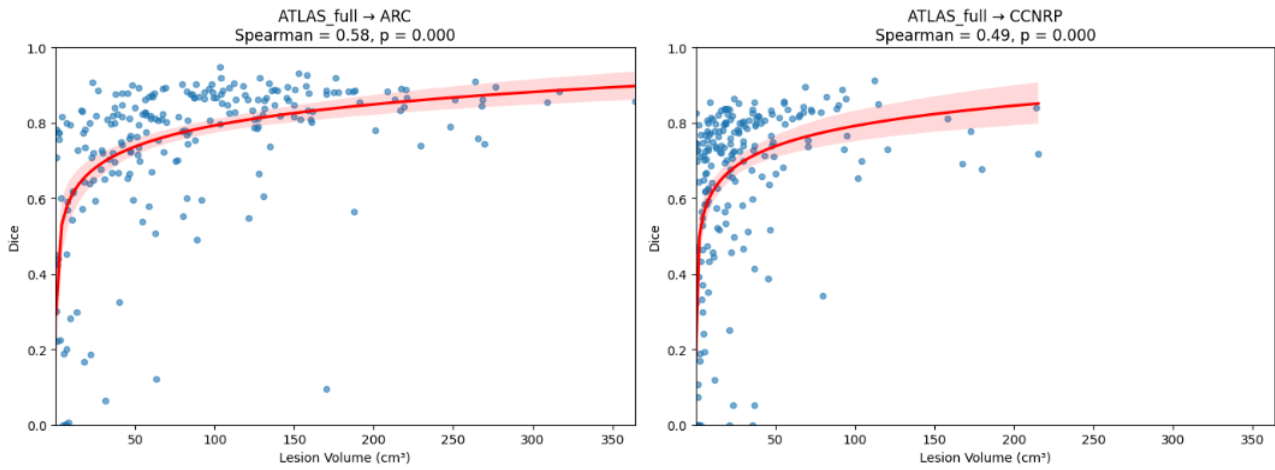


Figure 5. Correlation between lesion volume (cm^3) and segmentation accuracy for the ATLASv2-trained model. Scatterplots show the correlation between lesion volume (X-axis) and Dice coefficient (Y-axis) for predictions on the ARC dataset (left) and the CCNRP dataset (right). Curves depict nonlinear trend fits with 95% confidence intervals. Spearman correlation and corresponding p values are reported above each plot.

3.4.2 Training Set Effects: Small-Lesion Trained Models Generalise Poorly

To assess whether training on very small lesions improves generalisation to similar cases, we compared two models trained on volume-stratified ATLASv2 subsets: a small-lesion model (median = 1.14 cm^3 ; $n = 319$) and a large-lesion model (median = 34.01 cm^3 ; $n = 336$).

Internal validation revealed substantially poor performance for the small-lesion model compared to the large-lesion model (Dice = .56 vs. .82; $U = 20,780$, $p < .001$). While the large-lesion model generalised moderately to held-out small lesions (Dice = .54), the small-lesion model failed to generalise to larger lesions (Dice = .07). This asymmetry was amplified in external datasets. For ARC, the large-lesion model significantly outperformed the small-lesion model (Dice = .82 vs. .01; $U = 1,616$, $p < .001$), with a comparable pattern observed for CCNRP (Dice = .74 vs. .00; $U = 2,052$, $p < .001$).

3.4.3 Volume-Matched Analysis: Interactions of Training and Test Sets

The chronic datasets differed substantially in their lesion-volume distribution; therefore, we conducted a volume-matched analysis to isolate the contribution of lesion volume to cross-dataset generalisation. Lesion volume differed significantly across datasets (ARC > CCNRP > ATLASv2; all $p < .001$), motivating the construction of a subset of ATLASv2 ($n = 204$) whose lesion-volume distribution was statistically equivalent to CCNRP (3.95% vs. 4.08%; $U = 20,812$, $p > .05$).

Prior to matching, cross-dataset performance was asymmetric: the CCNRP-trained model performed poorly on the full ATLASv2 dataset (Dice = .50), whereas an ATLASv2-trained model generalised well to CCNRP (Dice = .73; asymmetry: $U = 10,940$, $p < .001$). When evaluation was restricted to the volume-matched ATLASv2 subset, this asymmetry was eliminated (CCNRP→ATLASv2_matched: Dice = .63; ATLASv2_matched→CCNRP: Dice = .66; $U = 20,140$, $p > .05$). This reflects a significant improvement of the CCNRP-trained model relative to its performance on the full ATLASv2 dataset ($U = 53,960$, $p < .001$), consistent with the matched subset containing larger, intrinsically easier to segment lesions. Conversely, the volume-matched ATLASv2-trained model exhibited slightly reduced performance on CCNRP relative to the full ATLASv2 model ($U = 24,682$, $p = .001$), likely reflecting reduced exposure to smaller lesions during training.

3.5 Image Quality Effect (chronic lesions; T1w)

To assess whether MRI image quality contributed to differences in model performance, we extracted T1w image quality metrics using MRIQC (Esteban et al., 2017). Metrics with very low variance across participants (< 0.01 after standardisation) were excluded, as they provided minimal discriminative information. We also removed sets of redundant metrics capturing overlapping information (e.g., axis-specific smoothness metrics `fmwhm_x`, `fmwhm_y`, `fmwhm_z`, which were redundant with the global smoothness estimate, `fmwhm_avg`). Finally, all metrics were recoded such that higher values reflected better image quality. A varimax rotated PCA produced a five-component solution with eigenvalues > 1 , explaining 83.1% of the total variance. Variables with absolute loading greater than 0.60 were interpreted for each component. The full component loading matrix is provided in Supplementary Material Table S2. Briefly, Factor 1 primarily reflected signal integrity, driven by SNR loadings across tissue classes. Factor 2 captured tissue-segmentation precision, dominated by residual partial volume

estimates. Factor 3 reflected spatial resolution and tissue contrast, combining positive loading for WM contrast and negative loading for spatial blurring. Factor 4 indexed signal consistency, with positive contributions from GM/CSF intensities. Factor 5 represented background contrast-to-noise characteristics, driven by CNR and background intensity measures.

A Kruskal–Wallis test revealed significant differences between datasets across all five components ($H = 7.48\text{--}397.88$, all $p < .05$). Follow-up Mann–Whitney U tests with Bonferroni correction showed that ARC scored significantly lower than both ATLAS and CCNRP on Factors 1, 2 and 4 (all p 's $< .001$), corresponding to reduced SNR, poorer tissue boundary definition, and less homogenous signal. ARC also scored lower than CCNRP on Factor 5 ($U = 26,281$, $p = .05$), reflecting weaker contrast-to-noise ratio and noisy background. In contrast, ARC scored significantly higher than other datasets on Factor 3 ($U = 4,578\text{--}93,509$, all $p < .001$), a dimension characterised by complex positive and negative loadings which made it less transparent to interpret. Standardised factor profiles across datasets are visualised in Figure 6.

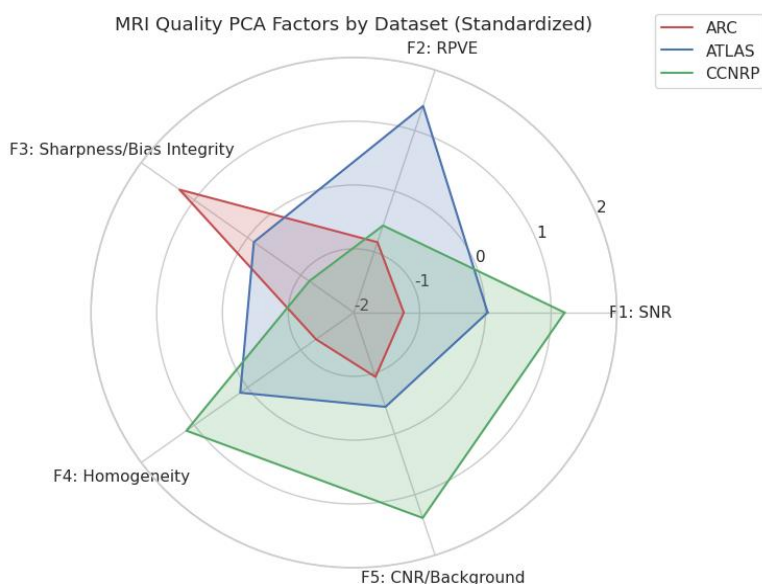


Figure 6. Standardized MRI quality factor scores by dataset.

Labels indicate the loading values for each variable within a factor. SNR = signal-to-noise ratio; RPVE = residual partial volume effect; CNR = contrast-to-noise ratio. Several MRIQC metrics were inverted prior to analysis so that higher values reflect better image quality. Accordingly, higher scores on Factors 1, 2, 4, and 5 indicate better quality. Factor 3 reflects a mixture of opposing loadings and therefore does not map linearly onto overall image quality.

4. Discussion

Reliable and scalable lesion segmentation is a cornerstone of stroke neuroscience, with direct implications for research, clinical prognosis, and personalised care (Kristinsson et al., 2021; C. F. Liu et al., 2023; Luo et al., 2024; Price, 2010). In this study, we systematically evaluated the performance and generalisability of the nnU-Net framework across multiple heterogeneous acute and chronic stroke MRI datasets. The best-performing models for acute (median = .78) and chronic (median = .73-.81) demonstrated robust external generalisation. These values fall within, and in some cases exceed, reported inter-rater reliability for manual annotations (Liew et al., 2018; Lo et al., 2022), highlighting the promise of automated approaches for large-scale research and as a foundation for future clinical deployment.

At the same time, segmentation performance varied systematically as a function of training data composition, lesion characteristics and image quality. Below, we situate these findings within the existing literature, discuss their implications, and outline challenges and opportunities for advancing toward clinically robust lesion segmentation.

Acute Lesion Models: DWI vs. FLAIR

For acute stroke, models trained on DWI consistently generalised well to independent datasets, whereas FLAIR-based models performed substantially worse. Combining FLAIR with DWI produced minimal gains and, in some cases, reduced accuracy relative to DWI alone. These findings are consistent with prior reports suggesting limited added value of FLAIR (Zhu et al., 2021).

A plausible explanation lies in the well-characterised temporal evolution of stroke lesions across MRI sequences. In the hyperacute phase, restricted diffusion is evident on DWI (high signal with low ADC), while FLAIR signal often remains normal, producing the classic DWI–FLAIR mismatch. Over subsequent days, lesions typically appear hyperintense on both DWI and FLAIR, with continued ADC reduction. By the subacute stage (1–3 weeks), DWI signal declines and ADC values pseudo-normalise, while FLAIR hyperintensity persists. Beyond this period, DWI becomes more variable with elevated ADC values (Hernandez Petzsche et al., 2022). Differences in acquisition timing between

datasets (SOOP <48 hours; ISLES 1-3 weeks) possibly contributed to variability in lesion appearance and influenced cross-data generalisation.

However, timing alone does not fully explain the poor performance of FLAIR-based models, which remained low even during internal validation. FLAIR images are inherently more variable, particularly in older populations, due to the frequent presence of white matter hyperintensities (WMH) and other chronic vascular changes that can obscure lesion boundaries and mimic infarcts (Debette & Markus, 2010; Gouw et al., 2011; Wardlaw et al., 2015). While FLAIR remains clinically valuable for estimating stroke onset (e.g., Thomalla et al., 2011), our findings indicate that DWI provides more reliable and discriminative features for acute and sub-acute lesion segmentation. Future work could explicitly model WMH as a separate class to disentangle chronic vascular pathology from acute ischemic injury.

More broadly, these modality-specific differences highlight a central challenge: stroke lesions are highly dynamic, with physiological and morphological changes unfolding across time. Visibility varies not only between sequences but also within the same sequence across stages (Hernandez et al., 2000). Models trained solely on acute-phase scans are therefore unlikely to generalise to chronic-stage lesions without explicitly accounting for lesion evolution. Next-generation approaches should aim to capture these temporal dynamics, enabling longitudinal and multimodal predictions.

Dataset Size During Training Matters

For chronic stroke, increasing training set size led to systematic performance gains, with the largest improvements observed when moving from small to medium datasets and more modest gains thereafter. This pattern aligns with broader findings in medical imaging, where performance improves with additional data until gains plateau (Bardis et al., 2020). Practically, our findings suggest that moderately sized but diverse datasets (~400–500 cases) can already support robust nnU-Net models for chronic T1w lesion segmentation. These diminishing returns likely reflect redundancy in homogeneous data rather than limits of model capacity, underscoring the importance of diversity over sheer sample size (Halevy et al., 2009).

Lesion laterality does not constrain generalisation

Despite marked differences in lesion laterality across datasets, laterality alone did not substantially limit generalisation. Models trained on left, right or bilateral lesions achieved comparable performance, and restricting training to unilateral lesions did not meaningfully degrade accuracy. These findings align with prior work suggesting that lesion volume, shape and anatomical dispersion are more critical determinants of segmentation accuracy than laterality (Abbasi et al., 2023; Soliman et al., 2024). The poor external performance of ARC-trained models therefore likely reflects other factors discussed below.

Lesion volume as key determinant of accuracy and generalisability

Lesion volume emerged as one of the strongest and most consistent predictors of segmentation performance (De Haan et al., 2015; Maier et al., 2015). Across all models and datasets, larger lesions were segmented more accurately, with strong positive correlations between lesion volume and Dice scores. Smaller lesions, particularly those below 20 cm³, were consistently more difficult to segment, consistent with previous reports (Abbasi et al., 2023; Luo et al., 2024; Zafari-Ghadim et al., 2024). This likely reflects subtle boundaries, greater anatomical variability, and lower tissue contrast – factors that also reduce inter-rater reliability in manual tracing (Ito et al., 2019).

Importantly, lesion volume also shaped generalisability through its representation in the training data. Models trained on small or large lesions generalised poorly outside their respective volume ranges, whereas models trained on broad volume distributions showed more symmetric cross-dataset performance. Volume-matching analyses further demonstrated that apparent generalisation asymmetries largely disappeared once lesion distributions were aligned.

Image Quality Matters

Differences in MRI quality also contributed to variation in generalisation. Using MRIQC-derived metrics summarised via PCA, we found that ARC exhibited systematically lower image quality across multiple dimensions, including SNR, tissue boundary definition, and signal homogeneity. These factors likely limited robust feature learning during training, despite reasonable internal accuracy (Esteva et al., 2017; Pizarro et al., 2016). Interestingly, ARC cases were segmented relatively well by models trained on higher-quality datasets, suggesting that training on diverse, high-quality data may confer some

robustness to lower-quality scans at inference. These findings align with broader machine-learning literature showing that low-quality training data can impair generalisation (Angluin & Laird, 1988; Frénay & Verleysen, 2016; Shorten & Khoshgoftaar, 2019).

Toward Clinical Translation

Although this study focused on MRI based segmentation, clinical translation ultimately requires consideration of real-world imaging workflows, particularly in acute stroke where CT remains the primary imaging modality. While CT offers lower soft-tissue contrast than MRI, segmentation may be enhanced using anatomical priors, tissue probability maps, and using multimodal CT–MRI datasets acquired within the same time window. Our findings motivate future work extending automated lesion segmentation to CT and multimodal clinical data.

Limitations

Several limitations should be acknowledged. Automated models are constrained by the quality and consistency of human-generated ground truth, which is known to be variable, particularly for small lesions (Ito et al., 2019). In some cases, model outputs appeared more anatomically coherent than the reference masks, highlighting ambiguity in the annotations rather than definitive model error. Future work may benefit from consensus-based labels, multi-rater probabilistic maps, or integrating vascular territory information (Zhao et al., 2020). Annotation protocols also introduce modality-specific bias. In both acute datasets, lesions were delineated primarily with reference to DWI, potentially disadvantaging FLAIR-based models. Sequence-specific annotations or multi-label approaches may better capture modality dependant lesion appearance. Finally, we did not exhaustively explore advanced multimodal architectures or pretraining strategies, which may leverage complementary information beyond the models tested here.

Conclusion

This study provides a comprehensive evaluation of automated stroke lesion segmentation using nnUNet across acute and chronic MRI datasets. We demonstrated robust external generalisation, with performance approaching human reliability, while identifying lesion volume, training data quality and dataset diversity as key determinants of accuracy. Acute segmentation benefits most from DWI, whereas chronic segmentation improves with moderate training set size before plateauing. Together,

these findings offer practical guidance for dataset curation and model development and outline a roadmap towards more robust, generalisable, and clinically relevant lesion segmentation.

All trained models and code are openly shared to promote transparency, reproducibility, and community benchmarking: (<https://github.com/AjayHalai/Lesion-Segmentation-nnUNet>).

References

- Abbasi, H., Orouskhani, M., Asgari, S., & Zadeh, S. S. (2023). Automatic brain ischemic stroke segmentation with deep learning: A review. *Neuroscience Informatics*, 3(4), 100145. <https://doi.org/10.1016/J.NEURI.2023.100145>
- Absher, J., Goncher, S., Newman-Norlund, R., Perkins, N., Yourganov, G., Vargas, J., Sivakumar, S., Parti, N., Sternberg, S., Teghipco, A., Gibson, M., Wilson, S., Bonilha, L., & Rorden, C. (2024). The stroke outcome optimization project: Acute ischemic strokes from a comprehensive stroke center. *Scientific Data* 2024 11:1, 11(1), 839-. <https://doi.org/10.1038/s41597-024-03667-5>
- Ahmed, R., Al Shehhi, A., Werghi, N., & Seghier, M. L. (2024). Segmentation of stroke lesions using transformers-augmented MRI analysis. *Human Brain Mapping*, 45(11), e26803. <https://doi.org/10.1002/HBM.26803>
- Angluin, D., & Laird, P. (1988). Learning from noisy examples. *Machine Learning* 1988 2:4, 2(4), 343–370. <https://doi.org/10.1007/BF00116829>
- Baaklini, M., & Valdés Hernández, M. del C. (2025a). Deep learning for MRI-based acute and subacute ischaemic stroke lesion segmentation—a systematic review, meta-analysis, and pilot evaluation of key results. *Frontiers in Medical Technology*, 7, 1491197. [https://doi.org/10.3389/FMEDT.2025.1491197/FULL](https://doi.org/10.3389/FMEDT.2025.1491197)
- Baaklini, M., & Valdés Hernández, M. del C. (2025b). Deep learning for MRI-based acute and subacute ischaemic stroke lesion segmentation—a systematic review, meta-analysis, and pilot evaluation of key results. *Frontiers in Medical Technology*, 7, 1491197. [https://doi.org/10.3389/FMEDT.2025.1491197/FULL](https://doi.org/10.3389/FMEDT.2025.1491197)
- Bardis, M., Houshyar, R., Chantaduly, C., Ushinsky, A., Glavis-Bloom, J., Shaver, M., Chow, D., Uchio, E., & Chang, P. (2020). Deep Learning with Limited Data: Organ Segmentation Performance by U-Net. *Electronics* 2020, Vol. 9, Page 1199, 9(8), 1199. <https://doi.org/10.3390/ELECTRONICS9081199>
- Bates, E., Wilson, S. M., Saygin, A. P., Dick, F., Sereno, M. I., Knight, R. T., & Dronker, N. F. (2003). Voxel-based lesion–symptom mapping. *Nature Neuroscience* 2003 6:5, 6(5), 448–450. <https://doi.org/10.1038/NN1050>
- Bowren, M., Bruss, J., Manzel, K., Edwards, D., Liu, C., Corbetta, M., Tranel, D., & Boes, A. D. (2022). Post-stroke outcomes predicted from multivariate lesion-behaviour and lesion network mapping. *Brain*, 145(4), 1338–1353. <https://doi.org/10.1093/BRAIN/AWAC010>
- Chalcroft, L., Pappas, I., Price, C. J., & Ashburner, J. (2025). Synthetic Data for Robust Stroke Segmentation. *Machine Learning for Biomedical Imaging*, 3(August 2025), 317–346. <https://doi.org/10.59275/j.melba.2025-f3g6>
- Chauhan, S., Vig, L., De Filippo De Grazia, M., Corbetta, M., Ahmad, S., & Zorzi, M. (2019). A Comparison of Shallow and Deep Learning Methods for Predicting Cognitive Performance of Stroke Patients From MRI Lesion Images. *Frontiers in Neuroinformatics*, 13, 451990. [https://doi.org/10.3389/FNINF.2019.00053/BIBTEX](https://doi.org/10.3389/FNINF.2019.00053)
- Çiçek, Ö., Abdulkadir, A., Lienkamp, S. S., Brox, T., & Ronneberger, O. (2016). 3D U-Net: Learning Dense Volumetric Segmentation from Sparse Annotation. *Lecture Notes in Computer Science (Including Subseries Lecture Notes in Artificial Intelligence and Lecture Notes in Bioinformatics)*, 9901 LNCS, 424–432. https://doi.org/10.1007/978-3-319-46723-8_49
- De Haan, B., Clas, P., Juenger, H., Wilke, M., & Karnath, H. O. (2015). Fast semi-automated lesion demarcation in stroke. *NeuroImage: Clinical*, 9, 69–74. <https://doi.org/10.1016/j.nicl.2015.06.013>
- Debette, S., & Markus, H. S. (2010). The clinical importance of white matter hyperintensities on brain magnetic resonance imaging: systematic review and meta-analysis. *BMJ*, 341(7767), 288. <https://doi.org/10.1136/BMJ.C3666>
- DeMarco, A. T., & Turkeltaub, P. E. (2018). A multivariate lesion symptom mapping toolbox and examination of lesion-volume biases and correction methods in lesion-symptom mapping. *Human Brain Mapping*, 39(11), 4169–4182. <https://doi.org/10.1002/HBM.24289>
- Esteban, O., Birman, D., Schaer, M., Koyejo, O. O., Poldrack, R. A., & Gorgolewski, K. J. (2017). MRIQC: Advancing the automatic prediction of image quality in MRI from unseen sites. *PLOS ONE*, 12(9), e0184661. <https://doi.org/10.1371/JOURNAL.PONE.0184661>
- Esteva, A., Kuprel, B., Novoa, R. A., Ko, J., Swetter, S. M., Blau, H. M., & Thrun, S. (2017). Dermatologist-level classification of skin cancer with deep neural networks. *Nature* 2017 542:7639, 542(7639), 115–118. <https://doi.org/10.1038/nature21056>
- Fedorov, A., Beichel, R., Kalpathy-Cramer, J., Finet, J., Fillion-Robin, J. C., Pujol, S., Bauer, C., Jennings, D., Fennessy, F., Sonka, M., Buatti, J., Aylward, S., Miller, J. V., Pieper, S., & Kikinis, R. (2012). 3D Slicer as an image computing platform for the Quantitative Imaging Network. *Magnetic Resonance Imaging*, 30(9), 1323–1341. <https://doi.org/10.1016/J.MRI.2012.05.001>

- Feigin, V. L., Krishnamurthi, R. V., Theadom, A. M., Abajobir, A. A., Mishra, S. R., Ahmed, M. B., Abate, K. H., Mengistie, M. A., Wakayo, T., Abd-Allah, F., Abdulle, A. M., Abera, S. F., Mohammed, K. E., Abyu, G. Y., Asgedom, S. W., Atey, T. M., Betsu, B. D., Mezgebe, H. B., Tuem, K. B., ... Zaki, M. E. (2017). Global, regional, and national burden of neurological disorders during 1990–2015: a systematic analysis for the Global Burden of Disease Study 2015. *The Lancet Neurology*, 16(11), 877–897. [https://doi.org/10.1016/S1474-4422\(17\)30299-5](https://doi.org/10.1016/S1474-4422(17)30299-5)
- Frénay, B., & Verleysen, M. (2016). Reinforced Extreme Learning Machines for Fast Robust Regression in the Presence of Outliers. *IEEE Transactions on Cybernetics*, 46(12), 3351–3363. <https://doi.org/10.1109/TCYB.2015.2504404>
- Gibson, M., Newman-Norlund, R., Bonilha, L., Fridriksson, J., Hickok, G., Hillis, A. E., den Ouden, D. B., & Rorden, C. (2024). The Aphasia Recovery Cohort, an open-source chronic stroke repository. *Scientific Data* 2024 11:1, 11(1), 981-. <https://doi.org/10.1038/s41597-024-03819-7>
- Gouw, A. A., Seewann, A., Van Der Flier, W. M., Barkhof, F., Rozemuller, A. M., Scheltens, P., & Geurts, J. J. G. (2011). Heterogeneity of small vessel disease: a systematic review of MRI and histopathology correlations. *Journal of Neurology, Neurosurgery & Psychiatry*, 82(2), 126–135. <https://doi.org/10.1136/JNNP.2009.204685>
- Griffis, J. C., Allendorfer, J. B., & Szaflarski, J. P. (2016). Voxel-based Gaussian naïve Bayes classification of ischemic stroke lesions in individual T1-weighted MRI scans. *Journal of Neuroscience Methods*, 257, 97–108. <https://doi.org/10.1016/J.JNEUMETH.2015.09.019>
- Halevy, A., Norvig, P., & Pereira, F. (2009). The unreasonable effectiveness of data. *IEEE Intelligent Systems*, 24(2), 8–12. <https://doi.org/10.1109/MIS.2009.36>
- Hernandez, A. E., Martinez, A., & Kohnert, K. (2000). In Search of the Language Switch: An fMRI Study of Picture Naming in Spanish–English Bilinguals. *Brain and Language*, 73(3), 421–431. <https://doi.org/10.1006/BRLN.1999.2278>
- Hernandez Petzsche, M. R., de la Rosa, E., Hanning, U., Wiest, R., Valenzuela, W., Reyes, M., Meyer, M., Liew, S. L., Kofler, F., Ezhov, I., Robben, D., Hutton, A., Friedrich, T., Zarth, T., Bürkle, J., Baran, T. A., Menze, B., Broocks, G., Meyer, L., ... Kirschke, J. S. (2022). ISLES 2022: A multi-center magnetic resonance imaging stroke lesion segmentation dataset. *Scientific Data* 2022 9:1, 9(1), 762-. <https://doi.org/10.1038/s41597-022-01875-5>
- Iorga, M., Higgins, J., Caplan, D., Zinbarg, R., Kiran, S., Thompson, C. K., Rapp, B., & Parrish, T. B. (2021). Predicting language recovery in post-stroke aphasia using behavior and functional MRI. *Scientific Reports*, 11(1), 8419. <https://doi.org/10.1038/s41598-021-88022-z>
- Iqbal, S., Zeeshan, M., Mehmood, M., Khan, T., & Razzak, I. (2024). TESL-Net: A Transformer-Enhanced CNN for Accurate Skin Lesion Segmentation. *Proceedings - 2024 25th International Conference on Digital Image Computing: Techniques and Applications, DICTA 2024*, 313–320. <https://doi.org/10.1109/DICTA63115.2024.00054>
- Isensee, F., Jaeger, P. F., Kohl, S. A. A., Petersen, J., & Maier-Hein, K. H. (2020). nnU-Net: a self-configuring method for deep learning-based biomedical image segmentation. *Nature Methods* 2020 18:2, 18(2), 203–211. <https://doi.org/10.1038/S41592-020-01008-Z>
- Ito, K. L., Kim, H., & Liew, S. L. (2019). A comparison of automated lesion segmentation approaches for chronic stroke T1-weighted MRI data. *Human Brain Mapping*, 40(16), 4669–4685. <https://doi.org/10.1002/HBM.24729>
- Jeong, H., Lim, H., Yoon, C., Won, J., Lee, G. Y., de la Rosa, E., Kirschke, J. S., Kim, B., Kim, N., & Kim, C. (2024). Robust Ensemble of Two Different Multimodal Approaches to Segment 3D Ischemic Stroke Segmentation Using Brain Tumor Representation Among Multiple Center Datasets. *Journal of Imaging Informatics in Medicine* 2024 37:5, 37(5), 2375–2389. <https://doi.org/10.1007/S10278-024-01099-6>
- Kristinsson, S., Zhang, W., Rorden, C., Newman-Norlund, R., Basilakos, A., Bonilha, L., Yourganov, G., Xiao, F., Hillis, A., & Fridriksson, J. (2021). Machine learning-based multimodal prediction of language outcomes in chronic aphasia. *Human Brain Mapping*, 42(6), 1682–1698. <https://doi.org/10.1002/HBM.25321>
- Liew, S. L., Lo, B. P., Donnelly, M. R., Zavaliangos-Petropulu, A., Jeong, J. N., Barisano, G., Hutton, A., Simon, J. P., Juliano, J. M., Suri, A., Wang, Z., Abdullah, A., Kim, J., Ard, T., Banaj, N., Borich, M. R., Boyd, L. A., Brodtmann, A., Buetefisch, C. M., ... Yu, C. (2022). A large, curated, open-source stroke neuroimaging dataset to improve lesion segmentation algorithms. *Scientific Data* 2022 9:1, 9(1), 320-. <https://doi.org/10.1038/s41597-022-01401-7>
- Liew, S.-L., Anglin, J. M., Banks, N. W., Sondag, M., Ito, K. L., Kim, H., Chan, J., Ito, J., Jung, C., Khoshab, N., Lefebvre, S., Nakamura, W., Saldana, D., Schmiesing, A., Tran, C., Vo, D., Ard, T., Heydari, P., Kim, B., ... Stroud, A. (2018). Data Descriptor: A large, open source dataset of stroke anatomical brain images and manual lesion segmentations. <https://doi.org/10.1038/sdata.2018.11>

- Liu, C. F., Leigh, R., Johnson, B., Urrutia, V., Hsu, J., Xu, X., Li, X., Mori, S., Hillis, A. E., & Faria, A. V. (2023). A large public dataset of annotated clinical MRIs and metadata of patients with acute stroke. *Scientific Data* 2023 10:1, 10(1), 1–14. <https://doi.org/10.1038/S41597-023-02457-9>
- Liu, L., Kurgan, L., Wu, F. X., & Wang, J. (2020). Attention convolutional neural network for accurate segmentation and quantification of lesions in ischemic stroke disease. *Medical Image Analysis*, 65, 101791. <https://doi.org/10.1016/J.MEDIA.2020.101791>
- Lo, B. P., Donnelly, M. R., Barisano, G., & Liew, S. L. (2022). A standardized protocol for manually segmenting stroke lesions on high-resolution T1-weighted MR images. *Frontiers in Neuroimaging*, 1, 1098604. <https://doi.org/10.3389/FNIMG.2022.1098604/FULL>
- Luo, X., Yang, Y., Yin, S., Li, H., Shao, Y., Zheng, D., Li, X., Li, J., Fan, W., Li, J., Ban, X., Lian, S., Zhang, Y., Yang, Q., Zhang, W., Zhang, C., Ma, L., Luo, Y., Zhou, F., ... Xie, C. (2024). Automated segmentation of brain metastases with deep learning: A multi-center, randomized crossover, multi-reader evaluation study. *Neuro-Oncology*, 26(11), 2140–2151. <https://doi.org/10.1093/NEUONC/NOAE113>
- Maier, O., Schröder, C., Forkert, N. D., Martinetz, T., & Handels, H. (2015). Classifiers for Ischemic Stroke Lesion Segmentation: A Comparison Study. *PLOS ONE*, 10(12), e0145118. <https://doi.org/10.1371/JOURNAL.PONE.0145118>
- Nazari-Farsani, S., Nyman, M., Karjalainen, T., Bucci, M., Isojärvi, J., & Nummenmaa, L. (2020). Automated segmentation of acute stroke lesions using a data-driven anomaly detection on diffusion weighted MRI. *Journal of Neuroscience Methods*, 333, 108575. <https://doi.org/10.1016/J.JNEUMETH.2019.108575>
- Pizarro, R. A., Cheng, X., Barnett, A., Lemaitre, H., Verchinski, B. A., Goldman, A. L., Xiao, E., Luo, Q., Berman, K. F., Callicott, J. H., Weinberger, D. R., & Mattay, V. S. (2016). Automated quality assessment of structural magnetic resonance brain images based on a supervised machine learning algorithm. *Frontiers in Neuroinformatics*, 10, 201996. <https://doi.org/10.3389/FNINF.2016.00052/BIBTEX>
- Price, Cathy. J. (2010). The anatomy of language: a review of 100 fMRI studies published in 2009. *Annals of the New York Academy of Sciences*, 1191(1), 62–88. [10.1111/j.1749-6632.2010.05444.x](https://doi.org/10.1111/j.1749-6632.2010.05444.x)
- Pustina, D., Coslett, H. B., Turkeltaub, P. E., Tustison, N., Schwartz, M. F., & Avants, B. (2016). Automated segmentation of chronic stroke lesions using LINDA: Lesion identification with neighborhood data analysis. *Human Brain Mapping*, 37(4), 1405–1421. <https://doi.org/10.1002/HBM.23110>
- Ronneberger, O., Fischer, P., & Brox, T. (2015). U-Net: Convolutional Networks for Biomedical Image Segmentation. *Lecture Notes in Computer Science (Including Subseries Lecture Notes in Artificial Intelligence and Lecture Notes in Bioinformatics)*, 9351, 234–241. https://doi.org/10.1007/978-3-319-24574-4_28
- Rorden, C., & Brett, M. (2000). Stereotaxic Display of Brain Lesions. *Behavioural Neurology*, 12(4), 191–200. <https://doi.org/10.1155/2000/421719>
- Seghier, M. L., Ramlackhansingh, A., Crinion, J., Leff, A. P., & Price, C. J. (2008). Lesion identification using unified segmentation-normalisation models and fuzzy clustering. *NeuroImage*, 41(4), 1253–1266. <https://doi.org/10.1016/J.NEUROIMAGE.2008.03.028>
- Sharma, N., Ray, A. K., Shukla, K. K., Sharma, S., Pradhan, S., Srivastva, A., & Aggarwal, L. (2010). Automated medical image segmentation techniques. *Journal of Medical Physics*, 35(1), 3–14. <https://doi.org/10.4103/0971-6203.58777>
- Shorten, C., & Khoshgoftaar, T. M. (2019). A survey on Image Data Augmentation for Deep Learning. *Journal of Big Data* 2019 6:1, 6(1), 60-. <https://doi.org/10.1186/S40537-019-0197-0>
- Soliman, A., Zafari-Ghadim, Y., Yousif, Y., Ibrahim, A., Mohamed, A., Rashed, E. A., & Mabrok, M. A. (2024). Deep models for stroke segmentation: do complex architectures always perform better? *IEEE Access*, 12, 198262–198276. <https://doi.org/10.1109/ACCESS.2024.3522214>
- Taha, A. A., & Hanbury, A. (2015). Metrics for evaluating 3D medical image segmentation: analysis, selection, and tool. *BMC Medical Imaging* 2015 15:1, 15(1), 29-. <https://doi.org/10.1186/S12880-015-0068-X>
- Thomalla, G., Cheng, B., Ebinger, M., Hao, Q., Tourdias, T., Wu, O., Kim, J. S., Breuer, L., Singer, O. C., Warach, S., Christensen, S., Treszl, A., Forkert, N. D., Galinovic, I., Rosenkranz, M., Engelhorn, T., Köhrmann, M., Endres, M., Kang, D. W., ... Gerloff, C. (2011). DWI-FLAIR mismatch for the identification of patients with acute ischaemic stroke within 4·5 h of symptom onset (PRE-FLAIR): A multicentre observational study. *The Lancet Neurology*, 10(11), 978–986. [https://doi.org/10.1016/S1474-4422\(11\)70192-2](https://doi.org/10.1016/S1474-4422(11)70192-2)
- Wardlaw, J. M., Valdés Hernández, M. C., & Muñoz-Maniega, S. (2015). What are white matter hyperintensities made of? Relevance to vascular cognitive impairment. *Journal of the American Heart Association*, 4(6), 001140. <https://doi.org/10.1161/JAHA.114.001140;ISSUE:ISSUE:DOI>
- Wilson, S. M., Entrup, J. L., Schneck, S. M., Onuscheck, C. F., Levy, D. F., Rahman, M., Willey, E., Casilio, M., Yen, M., Brito, A. C., Kam, W., Davis, L. T., De Riesthal, M., & Kirshner, H. S. (2023). Recovery from aphasia in the first year after stroke. *Brain*, 146(3), 1021–1039. <https://doi.org/10.1093/BRAIN/AWAC129>

- Yushkevich, P. A., & Gerig, G. (2017). ITK-SNAP: An Intractive Medical Image Segmentation Tool to Meet the Need for Expert-Guided Segmentation of Complex Medical Images. *IEEE Pulse*, 8(4), 54–57. <https://doi.org/10.1109/MPUL.2017.2701493>
- Zafari-Ghadim, Y., Rashed, E. A., Mohamed, A., & Mabrok, M. (2024). Transformers-based architectures for stroke segmentation: a review. *Artificial Intelligence Review* 2024 57:11, 57(11), 307-. <https://doi.org/10.1007/S10462-024-10900-5>
- Zhang, Y., Kimberg, D. Y., Coslett, H. B., Schwartz, M. F., & Wang, Z. (2014). Multivariate lesion-symptom mapping using support vector regression. *Human Brain Mapping*, 35(12), 5861–5876. <https://doi.org/10.1002/HBM.22590>
- Zhao, R., Qian, B., Zhang, X., Li, Y., Wei, R., Liu, Y., & Pan, Y. (2020). Rethinking dice loss for medical image segmentation. *Proceedings - IEEE International Conference on Data Mining, ICDM, 2020-November*, 851–860. <https://doi.org/10.1109/ICDM50108.2020.00094>
- Zhu, H., Jiang, L., Zhang, H., Luo, L., Chen, Y., & Chen, Y. (2021). An automatic machine learning approach for ischemic stroke onset time identification based on DWI and FLAIR imaging. *NeuroImage: Clinical*, 31, 102744. <https://doi.org/10.1016/J.NICL.2021.102744>

Supplementary Materials

Supplementary materials are available at
[GitHub - AjayHalai/Lesion-Segmentation-nnUNet](https://github.com/AjayHalai/Lesion-Segmentation-nnUNet)